Investigations on aerosol transport and deposition behavior during severe reactor accident

HOSAN, Md. Iqbal
Department of Applied Quantum Physics and Nuclear Engineering, Kyushu University

TAKANISHI, Kohei
Department of Applied Quantum Physics and Nuclear Engineering, Kyushu University

MORITA, Koji
Department of Applied Quantum Physics and Nuclear Engineering, Kyushu University

LIU, Wei
Department of Applied Quantum Physics and Nuclear Engineering, Kyushu University

他

出版情報：Mechanical Engineering Journal. 11 (2), pp.23-00423-, 2024. 日本機械学会
バージョン：

Bulletin of the JSME Vol.11, No.2, 2024
Mechanical Engineering Journal

Investigations on aerosol transport and deposition behavior during severe reactor accident

Md. Iqbal HOSAN*,**, Kohei TAKANISHI*, Koji MORITA*, Wei LIU* and Xu CHENG***
*Department of Applied Quantum Physics and Nuclear Engineering, Kyushu University
744 Motooka, Nishi-ku, Fukuoka 819-0395, Japan
E-mail: hosan.md.iqbal.929@s.kyushu-u.ac.jp
**Department of Nuclear Engineering, University of Dhaka
Nilkhet Road, Dhaka 1000, Bangladesh
***Institute of Applied Thermofluidics, Karlsruhe Institute of Technology
Street 3, Vincenz-Priessnitz, Karlsruhe 76131, Germany

Received: 4 October 2023; Revised: 24 December 2023; Accepted: 20 February 2024

Abstract
The accident at the Fukushima Daiichi Nuclear Power Plant in 2011 led to a core meltdown, resulting in the significant release of radioactive materials into the environment, revealing the urgent need for further in-depth development of Level 2 probabilistic safety assessment technology. To help establish an effective source-term migration evaluation method, this study investigates fission product migration behavior across leak pathways. Specifically, an experimental line is developed, and experiments are performed under conditions that simulate the environmental and flow conditions in containment vessel penetrations and failure locations during a severe accident. The experiments are conducted in narrow circular pipes, which represent the leak pathways in the containment vessel and reactor building, to determine the impact of flow rate, particle size, and flow path size on the decontamination factors. Additionally, a turbulent deposition model that accounts for re-entrainment effects has been developed, and the experimentally obtained decontamination factors are compared with the developed model, as well as a conventional model. The predicted decontamination factors from the present model exhibit similar trends and values to the experimental results.

Keywords: Severe reactor accident, Source term, Decontamination factor, Re-entrainment, Transport behavior, Aerosol particle, Deposition rate

1. Introduction

Nuclear Power plants (NPPs) provide a significant contribution to global energy generation, addressing the growing energy demands of modern societies. However, severe accidents (SA) in these facilities can have significant consequences, including the release of radioactive materials into the environment, which can pose threats to human health and environmental safety. The Fukushima Daiichi NPP accident occurred on March 11, 2011, resulting in a core meltdown and the release of radioactive materials into the environment. The study of SAs and the development of core damage assessment technology, especially the Level 2 probabilistic safety assessment have gained more attention since this accident. The Level 2 probabilistic safety assessment is used to analyze accidents in NPPs, identify ways in which radioactive materials may be released from plants, and estimate the release magnitude and frequency (Zvoncek et al., 2017).

When SAs occur at NPPs, radioactive fission products (FPs) are generated within the reactor pressure vessel and can be released into the environment through electrical penetrations, ducts, pores, and cracks that develop in the containment vessel (CV) (Allelein et al., 2009; Lin et al., 2015). The quantity of radioactive FPs released to the environment is referred to as the source term and is influenced by both the severity of the accident and the prevailing physical and chemical conditions. The transport of aerosols through these leakages is contingent on various factors

Paper No.23-00423
J-STAGE Advance Publication date : 1 March, 2024
[DOI: 10.1299/mej.23-00423]

such as pressure differentials across the leakage, aerosol concentrations, particle size distributions, dimensions of leakage pathways, and flow rates (Narayanam et al., 2020). To advance the Level 2 probabilistic safety assessment technology and mitigate the potential impact of SAs, it is imperative to gain a comprehensive understanding of the transport and deposition behavior of the accidental source terms.

Several studies have investigated the transport of aerosols through various types of leakage pathways and their dependence on pressure, humidity, path size, mass concentration, and aerosol size. In Japan, large-scale experiments were performed at the Nuclear Power Engineering Center on actual components of a CV in a boiling water reactor, which had been damaged by heating and pressurization, using dry CsI aerosol particles (Watanabe et al., 2009). The decontamination factors (DFs) obtained in these tests ranged between 10 and 1000 (Parozzi et al., 2005). Additionally, the penetration of potassium chloride aerosols under laminar flow through different air leakage pathways and cracks has been examined in common building materials such as aluminum, brick, and concrete (Liu and Nazaroff, 2003). Other studies have considered the clogging effect of aerosol particles in duct piping (Morewitz, 1982), and obtained DF data involving small concrete cracks (Vate, 1988). Although source-term migration studies have revealed some insights into aerosol transport, wide variations have been observed in the DF data. Furthermore, the mechanisms governing aerosol migration remain unclear, and there is a lack of reports on the modeling of these phenomena.

Aerosol particle deposition in turbulent flow through a pipe has previously been investigated based on the free flight model (FFM) (Friedlander and Johnstone, 1957). According to the FFM, if a particle flies within one stopping distance (S) from the wall, then it freely flies to the tube wall and deposits, as illustrated in Fig. 1. Particle inertia was considered the predominant deposition mechanism, and it was assumed that the particle and carrier gas diffusivities were identical. Brownian diffusion was neglected and deposition due to gravity was not included in the Friedlander and Johnstone (1957) model.

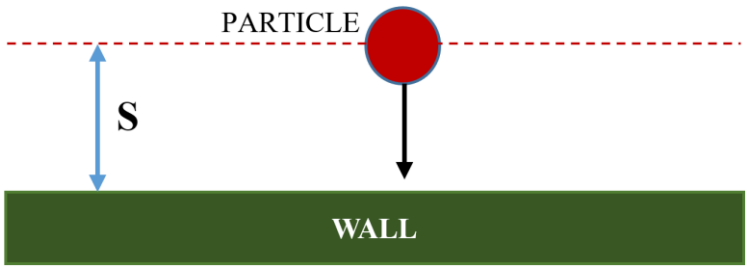

Fig. 1 Illustration of the deposition process that occurs in the FFM, where a particle freely falls toward the wall surface.

To predict the deposition velocity of aerosol flow through a horizontal pipe under turbulent flow conditions, Matsui and Murata's (1992) model has been used in various applications. The model is based on the FFM but considers the effective particle diffusion coefficient defined by Liu and Ilori (1974). Matsui and Murata (1992) determined a relationship between the deposition velocity V_1 and DF for a circular pipe of length L, diameter D_e, and fluid flowing through the pipe with a velocity u, which is expressed in Eq. (1).

$$DF = \frac{1}{exp(-4 V_1 L / u D_e)} \tag{1}$$

The Matsui and Murata (1992) model does not account for the re-entrainment of the deposited aerosol particles. According to this model, when a particle reaches the stopping distance, it permanently becomes attached to the wall (i.e., when a particle reaches the wall, it can never be re-entered into the main flow). However, in most practical problems, the deposition and re-entrainment of aerosols occur simultaneously. Several studies have considered the particle re-entrainment occurring after deposition on the wall surfaces, and several models have been presented to explain the mechanism of re-entrainment (Adhiwidjaja et al., 2000; Matsusaka and Masuda, 1996; Zhu et al., 2012). The development of an effective aerosol deposition and re-entrainment model is crucial for designing and optimizing the safety systems in NPPs, as well as estimating their performance and efficiency.

[DOI: 10.1299/mej.23-00423]

The present study aims to obtain fundamental data regarding the deposition of FPs, particularly dry aerosols, in narrow circular pipes under turbulent flow, which are used to simulate CV penetrations. Then, we evaluate the influence of particle size, Reynolds number (flow rate), and leakage path dimensions on DFs. Finally, the aerosol deposition model is developed considering the re-entrainment effect, specifically for turbulent flow through a horizontal channel.

2. Experimental measurement of DF

2.1 Experimental setup

The basic environmental components in the CV are air, water vapor, hydrogen, and other gases. In this study, nitrogen gas is used as a carrier gas of aerosol particles (i.e., silica) because the viscous resistance is similar to air. Figure 2 depicts the schematic of the experimental setup. Nitrogen gas, which is provided by a nitrogen gas cylinder, is delivered into two streams. One goes to an atomizer, where wet aerosol is produced, and the other goes to a drying section, where the wet aerosol comes out of the atomizer and is dried. A compact single-jet atomizer is used for generating and spraying the wet aerosol into the drying section. In the atomizer, aerosol particles are suspended in ethanol. A magnetic rotor is used to agitate the aerosol particles and ensure that all particles are dispersed and suspended well in the ethanol. The moist aerosol from the atomizer is dried at the drying section by the nitrogen gas from the gas cylinder. The dried aerosol in the drying section is branched into two channels. One passes through a filter and is released into the atmosphere, and the other flows into the test section with the suction of a vacuum pump. Note that the atmospheric release line is used here for the safety of the atomizer. The flow rate in the line of the test section is adjusted and measured using needle valves and mass flowmeters.

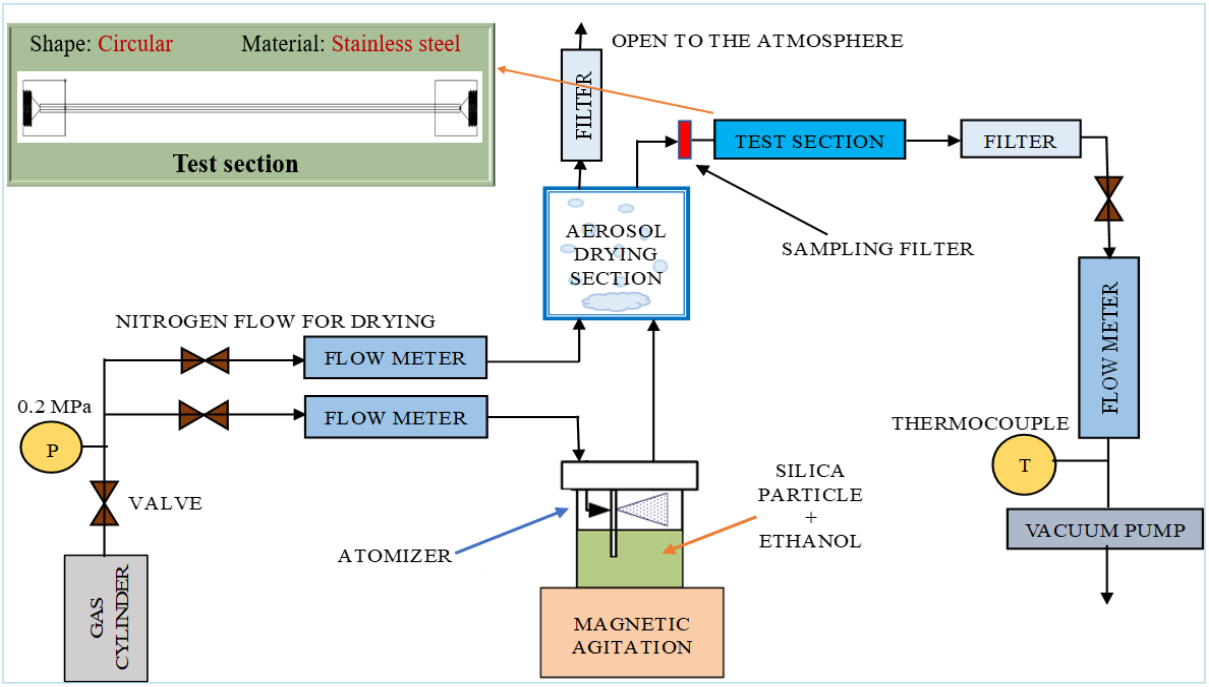

Fig. 2 Schematic of the experimental setup and narrow circular pipe test section used to obtain the FP deposition data.

2.2 Test section and experimental conditions

This study considers leakage pathways involving damaged organic seals at electrical wire penetrations or between organic seals and the pipe body. The shape of such a leak developed during an SA can be either complicated or relatively straight. In this study, the straight-through type is considered in a stainless-steel pipe because it has the lowest DF. The length of the test section depends on the shape of the organic sealant breakage and the type of electrical wiring penetration. Based on the filling length of the organic sealant in electrical wiring penetrations, the test section is 200

[DOI: 10.1299/mej.23-00423]

and 250 mm. The leakage path size depends on the size of the damage created in the organic sealant. In this study, the inner diameter of the pipe is 1.0 and 2.0 mm.

The different experimental conditions used in this study are listed in Table 1. The conditions are chosen to determine the impacts of flow path dimension, particle size, and flow rate on DFs.

Table 1 Different test cases and conditions

Effect	Case name	Pipe diameter (mm)	Length (mm)	Particle nominal diameter (μm)	Measured particle median diameter (μm)	Flow rate (l/min)
Particle size	C-D-1	1.0	250	0.5	3.6	4.0
	C-D-2			1.0	2.6	
	C-D-3	2.0		0.5	3.6	
	C-D-4			1.0	2.6	
Flow path size	C-S-1	1.0	200	1.0	2.6	4.0
	C-S-2	2.0				
	C-S-3	1.0	250			
	C-S-4	2.0				
Flow rate	C-F-1	1.0	250	1.0	2.6	3.0
	C-F-2					4.0
	C-F-3	2.0				4.0
	C-F-4					5.0

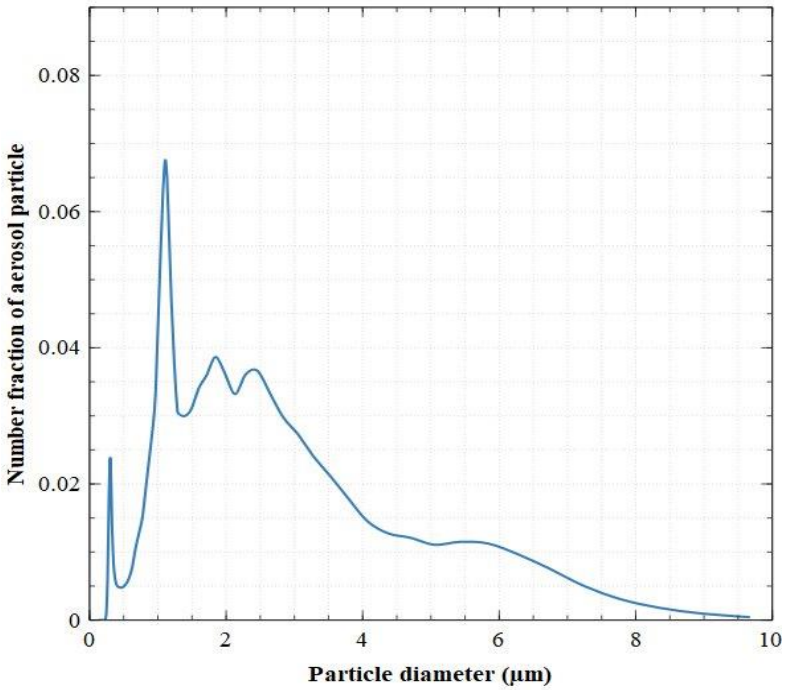

Fig. 3 Aerosol particle distribution fraction for a nominal particle size of 1 μm and a flow rate of 5 l/min.

In a typical boiling water reactor, Cs, I, and Te are the most commonly found radioactive materials in the source term of an SA. The densities of major FPs (e.g., CsI, I_2, and CH_3I) are in the range of 2.28 to 4.93 g/cm^3. Although the chemical properties of the particles generally have little effect on the transport of aerosols, the density and size of the particles have a significant effect. In this research, silica is chosen with a density of approximately 2.2 g/cm^3, and the

[DOI: 10.1299/mej.23-00423]

generated aerosol has a size distribution of 0.1 to 10 μm. Furthermore, hygroscopicity is expected to have a significant effect on aerosol particle deposition and transport. Particles with a hygroscopic nature exhibit dynamic behaviors owing to their propensity to absorb moisture from the surroundings, leading to changes in their size, shape, and texture. However, our experiment is aimed at obtaining basic data under experimental conditions that exclude the effects of humidity. The use of silica, a non-hygroscopic particle, ensures minimal or negligible moisture absorption from the environment while supporting simplified modeling of aerosol behavior in deposition studies. Further studies are necessary to evaluate the effects of humidity and particle hygroscopicity.

In aerosol deposition experiments, aerosol particles may agglomerate or break up in the process of reaching the test section. As a result, the size distribution of the aerosol particles that reach the test section may differ from the nominal value of the particles. Therefore, the size distribution of the aerosol particles is evaluated in this experiment using an aerosol spectrometer (Welas digital 2000, PALAS GmbH) placed at the inlet position of the test section. Figure 3 shows an example of the aerosol particle distribution fraction for a nominal particle size of 1 μm and a flow rate of 5 l/min.

2.3 Experimental procedure

For each experimental case, two experiments are carried out: one to measure the particle concentration at the inlet of the test section and the other to measure the particle concentration at the outlet of the test section. For the inlet concentration measurement test, the sampling filter is connected before the test section, but for the outlet concentration measurement, the sampling filter is connected in the experimental line after the test section. The only difference between these two tests is the position of the sampling filter. The experiments were carried out in the following manner.

i. Set the sampling filter upstream of the test section and conduct the inlet concentration measurement test.
   - Measure the weight of the filter paper in the sampling filter using an electronic balance.
ii. Preparation of suspension solution
   - Put 5.0 g of particles into the container of the atomizer.
   - Add approximately 100 ml of ethanol into the container.
   - Place the container on top of a magnetic rotator to disperse the particles in ethanol.
   - Attach the head of the atomizer to the container and connect the head to the experimental line.
iii. Construct the experimental line using clean connectors and tubes.
iv. Start the nitrogen gas flow and the vacuum pump.
   - Adjust the test section flow rate to the desired value and run the measurement for 45 min.
v. After the measurement is complete, remove the filter paper from the sampling filter and measure the mass.
vi. Replace the used connecting tubes with new ones and clean and dry all the components used in the experiments.
vii. After weighing a new filter paper, set the sampling filter downstream of the test section and conduct the outlet concentration measurement test by repeating steps ii through v.

Source-term deposition and transport are quantitatively evaluated by measuring the DF, which is defined by Eq. (2).

$$DF = \frac{C_{in}}{C_{out}} \tag{2}$$

where C_{in} and C_{out} are the inlet and outlet mass concentrations, which are calculated using Eqs. 2(a) and 2(b), respectively.

$$C_{in} = \frac{\Delta M_{in}}{Q_{in} t_{in}} \tag{2a}$$

$$C_{out} = \frac{\Delta M_{out}}{Q_{out} t_{out}} \tag{2b}$$

[DOI: 10.1299/mej.23-00423]

where ΔM_{in} and ΔM_{out} denote the change in mass of the filter paper during the inlet and outlet concentration measurement tests, respectively. Q_{in} and Q_{out} are the flow rates in the inlet and the outlet concentration measurement tests, respectively, and t_{in} and t_{out} denote the test durations. The mass of the filter paper is measured using an electronic balance which has a measurement uncertainty (standard deviation) of ±0.2 mg, and the error in the filter mass increase is ±0.283 mg, which is √2 times that value from the law of error propagation.

2.4 Experimental results

To develop the evaluation method for studying the transport and deposition of accidental source terms during SAs, the basic data are experimentally measured herein. The inlet and outlet concentrations were calculated by measuring the change in mass of the filter paper after conducting the two experiments for each case. The experimentally measured DFs for various cases are summarized in Table 2.

Table 2 Experimentally measured DFs for various test cases.

Effect	Case name	Reynolds number (-)	C_{in} (μg/l)	C_{out} (μg/l)	Experimental DF (-)
Particle size	C-D-1	5240	154	52.9	2.91
		5212	33.2	16.2	2.05
	C-D-2	5664	160	70.4	2.27
		5419	125	64.9	1.93
	C-D-3	2718	162	109	1.49
		2740	135	101	1.34
	C-D-4	2899	123	91.2	1.35
		2648	186	155	1.20
Flow path size	C-S-1	6000	133	63.6	2.09
		5946	116	72.7	1.60
	C-S-2	2603	195	121	1.61
		2560	119	89.1	1.34
	C-S-3	5664	160	70.4	2.27
		5419	125	64.9	1.93
	C-S-4	2899	123	91.2	1.35
		2648	186	155	1.20
Flow rate	C-F-1	4163	174	50.8	3.42
		4212	119	57.9	2.06
	C-F-2	5664	160	70.4	2.27
		5419	125	64.9	1.93
	C-F-3	2899	123	91.2	1.35
		2648	186	155	1.20
	C-F-4	3230	176	93.6	1.89
		3382	117	74.4	1.57

To check the adaptability of Matsui and Murata's existing deposition model, the results obtained from the experiments and the model are plotted in Fig. 4. At lower Re numbers, the predicted values are relatively consistent with the experimental values, with similar orders of magnitude, affirming the reliability of the Matsui and Murata model. However, there is an observable disparity between the predicted and experimental results as the Re number increases. This discrepancy may be attributed to the significant re-entrainment of the aerosol particles at higher Re numbers. Matsui and Murata's model assumes that particles freely fly to the wall within a certain stopping distance and are permanently attached to the wall (i.e., when a particle reaches the wall, it is never re-entrained in the main flow).

[DOI: 10.1299/mej.23-00423]

However, the particles that reach the wall surface in the experiment may be re-entrained in the main flow. Because deposition and re-entrainment occur simultaneously, they must be considered in a single model.

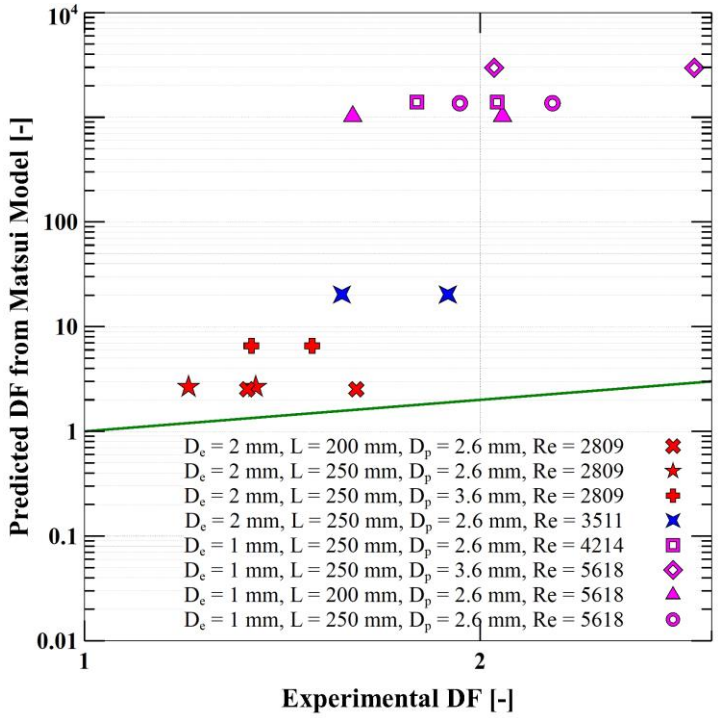

Fig. 4 Comparison of the experimentally measured DFs for different test cases and the predictions obtained from the Matsui and Murata model for the same conditions.

3. Development of a turbulent deposition model considering re-entrainment

The deposition and re-entrainment of aerosol particles under turbulent flow is illustrated in Fig. 5. During the flow of aerosol particles through a pipe, some particles are primarily deposited on the wall surface, and some may re-entrain from the surface into the main flow. The net number of particles that remain deposited on the wall is the difference between the particles moving toward the wall and the particles detaching from the wall, which is shown in Eq. (3).

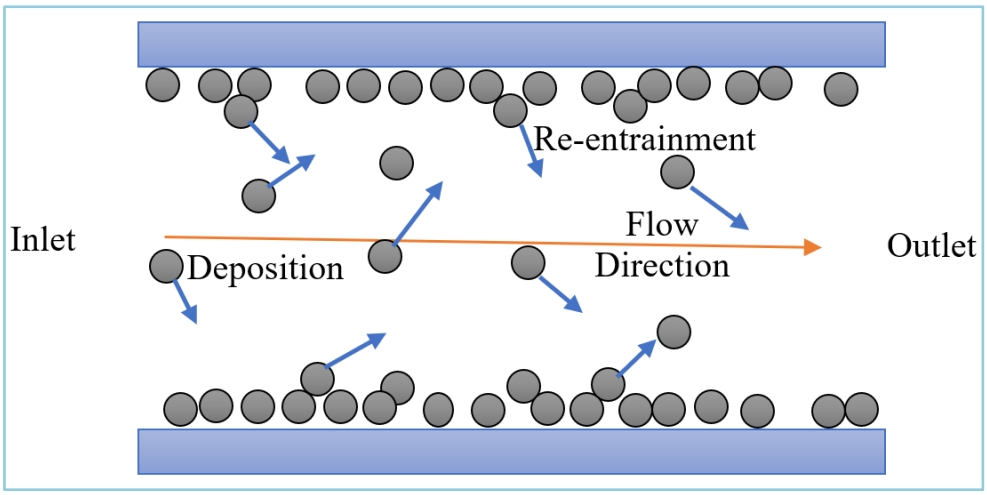

Fig. 5 Illustration of the deposition and re-entrainment of aerosol particles during turbulent flow in a circular pipe.

[DOI: 10.1299/mej.23-00423]

$$\varphi(\alpha)rd\alpha = \varphi_1(\alpha)rd\alpha - \varphi_2(\alpha)rd\alpha \tag{3}$$

where $\varphi(\alpha)$ is the net aerosol number flux at position (r, α) and $\varphi_1(\alpha)$ and $\varphi_2(\alpha)$ are the aerosol number deposition flux and re-entrainment flux, respectively. The deposition flux $\varphi_1(\alpha)$ in the free flight angular direction α, can be written according to Matsui and Murata (1992):

$$\varphi_1(\alpha) = \varepsilon_p \frac{dX(\alpha)}{dy} + v_g cos\alpha\, X(\alpha) \tag{4}$$

where $X(\alpha)$ is the particle concentration at distance y from the wall, and ε_p and v_g are the particle's effective turbulent diffusion coefficient and terminal settling velocity, respectively. The first part of the right side of Eq. (4) represents the deposition due to effective turbulent diffusion and the second part represents the deposition due to gravitational settling.

When particles are deposited, a deposition layer forms on the wall, but under the effect of re-entrainment, some fraction of the deposited particles may re-enter the main flow. The fraction of particles re-entrained into the main flow per unit surface area of the wall per unit time is defined as F. F is always ≤ 1. Then, the number of re-entrained particles from a unit surface area of the wall per unit of time (i.e., the re-entrainment flux $\varphi_2(\alpha)$) is expressed in Eq. (5).

$$\varphi_2(\alpha) = F * \varphi_1(\alpha) \tag{5}$$

Now, Eq. (3) becomes:

$$\varphi(\alpha) = (1\text{-}F)\, \varphi_1(\alpha) \tag{6}$$

Equation (6) can be written in terms of the effective deposition velocity, V, which comes from the combined effect of deposition and re-entrainment:

$$\int_0^{2\pi} \frac{\varphi(\alpha)}{X_{av}} = \int_0^{2\pi} (1\text{-}F) * \frac{\varphi_1(\alpha)}{X_{av}} \tag{7}$$

$$V = (1\text{-}F) * V_1 \tag{8}$$

where X_{av} is the average particle concentration and V_1 is the deposition velocity according to Matsui and Murata's (1992) model, which is calculated using Eq. (9).

$$V_1 = \frac{u^*}{2\pi} \begin{cases} \int_0^{2\pi} \dfrac{1}{exp\left(-\int_{\delta^+}^{b^+} M\, dy^+\right) * \int_{\delta^+}^{b^+} N * exp\left(\int_{\delta^+}^{y^+} M\, dy^+\right) dy^+} d\alpha\,; & (\delta^+ \le 30) \\ \int_0^{2\pi} \dfrac{1}{exp\left(-\int_{30}^{b^+} M\, dy^+\right) * \int_{30}^{b^+} N * exp\left(\int_{30}^{y^+} M\, dy^+\right) dy^+} d\alpha\,; & (\delta^+ > 30) \end{cases} \tag{9}$$

where u^* is the friction velocity, δ^+ is the dimensionless distance of the particle position to the tube wall, b^+ is the dimensionless radius of the pipe, and y^+ is the dimensionless distance from the pipe wall. M and N are defined in Eqs. (9a) and (9b), respectively.

$$M = \frac{v_g{}^+ cos\alpha}{\varepsilon_p{}^+} \tag{9a}$$

$$N = \frac{M}{v_g{}^+ cos\alpha} = 1/\varepsilon_p{}^+ \tag{9b}$$

where $v_g{}^+$ is dimensionless terminal setting velocity and $\varepsilon_p{}^+$ is dimensionless effective particle diffusion coefficient.

[DOI: 10.1299/mej.23-00423]

3.1 Fraction of re-entrainment flux calculation

To find the fraction F of the re-entrainment flux, we use the turbulent burst model proposed by Cleaver and Yates (1973). From detailed investigations of the turbulent boundary layer, it is found that the turbulent boundary layer is unsteady and continuously disrupted by bursts, which are essentially miniature tornados. The deposited particles detach from the wall surface and move into the main flow because of these turbulent bursts. This turbulent burst occurs randomly in the viscous sublayer, as close as $y^+ = 2.5$ from the wall surface.

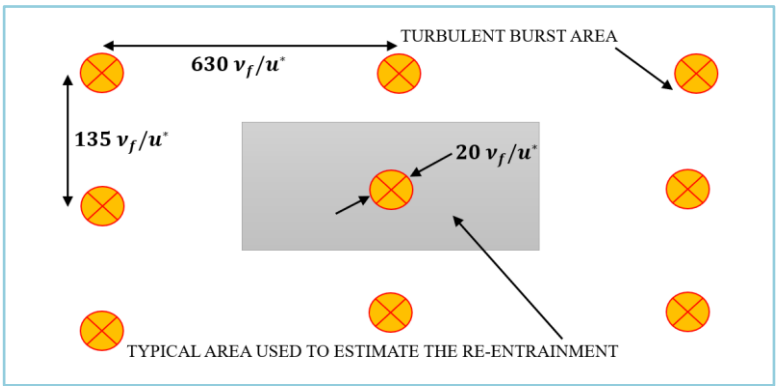

Fig. 6 Illustration of the distribution of turbulent bursts on the wall surface. The circles represent individual burst areas (Cleaver and Yates, 1973).

The theoretical distribution of the turbulent bursts is shown in Fig. 6. Cleaver and Yates (1973) assumed that each burst is circular, with a mean diameter $d_b = 20\frac{\nu_f}{u^*}$, where ν_f is the kinematic viscosity. The mean distances between two bursts in the axial and lateral directions are assumed to be $l_x = 630\frac{\nu_f}{u^*}$ and $l_y = 135\frac{\nu_f}{u^*}$, respectively. The typical area used to estimate the fraction of the re-entrainment flux is $(l_x l_y)$, and it is assumed that only one burst occurs at any one time within this area. The area fraction that is affected by the burst is expressed in Eq. (10).

$$\lambda = \frac{\pi d_b^2}{4 l_x l_y} \tag{10}$$

It is also assumed that the burst occurs consistently with time and the burst repeats after a time T.

$$T = 75\frac{\nu_f}{u^{*2}} \tag{11}$$

If the fraction of re-entrained particles from one burst is ξ, then the fraction of the re-entrainment flux on the typical area is expressed as follows:

$$F = \frac{\lambda \xi}{T} \tag{12}$$

Cleaver and Yates (1973) did not provide any method to directly calculate ξ. However, they pointed out that the value of ξ could be estimated based on the assumption that it is proportional to the wall shear stress. Thus, a semi-empirical expression was proposed to estimate the fraction of particles re-entrained from a turbulent burst (Zhu et al., 2012). The ξ is estimated as follows:

$$\xi = \frac{u^{*2}}{u_{th}^{*2}} \tag{13}$$

where u_{th}^* is the threshold friction velocity under which the particle starts to re-entrain under the effect of the turbulent burst. Based on Eq. (13), the fraction of the re-entrainment flux can be calculated using Eq. (14):

[DOI: 10.1299/mej.23-00423]

$$F = \frac{\lambda\, u^{*4}}{75\, \nu_f\, u_{th}^{*2}} \tag{14}$$

When a particle is deposited on a wall, it can easily form an aggregate, as shown in Fig. 7. The aggregate is submerged within the viscous sublayer of the flow at the wall, which has a velocity distribution u(y) proportional to the distance y from the wall, where the turbulent burst occurs. The diameter of the aggregate particles D_{ag} is calculated using Eq. (15), and four types of force are considered: the (i) adhesion force F_a between the particle and wall, (ii) gravitational force F_g, (iii) drag force F_d, and (iv) collision-induced force F_c. The first two forces attract the aggregate to the wall and the other two forces separate the aggregate from the wall.

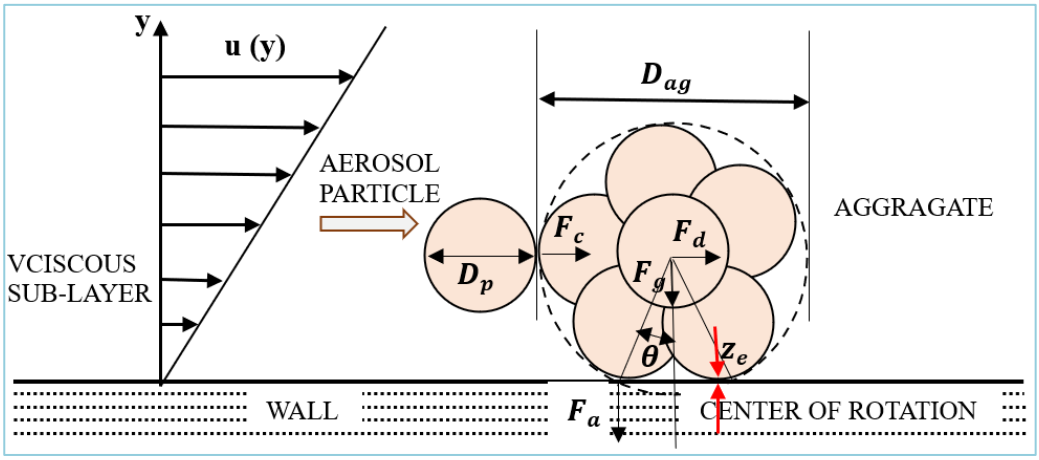

Fig. 7 Illustration of the different forces acting on the aerosol particle or the aggregate within the viscous sublayer (Theerachaisupakij et al., 2003).

$$D_{ag} = k_0\, D_p \tag{15}$$

where k_0 is a constant and D_p is particle diameter.

When the particle net separation moment exceeds the adhesion moment, the particle re-entrains into the main flow. The threshold re-entrainment velocity can be obtained from Eq. (16) (Kousaka et al., 1980; Matsusaka and Masuda, 1996; Theerachaisupakij et al., 2003):

$$k_1 D_p u_{th}^{7/4} + k_2 D_p^{11/5} u_{th}^{21/10} = 1 \tag{16}$$

where u_{th} is the average flow velocity in the pipe corresponding to the threshold friction velocity, referred to as the threshold re-entrainment velocity, and k_1 and k_2 are defined as follows:

$$k_1 = 1.40\, A^{-1} z_e^2 \upsilon_f^{\frac{1}{4}} D_e^{-\frac{1}{4}} \rho_f k_0^2 \operatorname{cosec}\theta \tag{16a}$$

$$k_2 = 0.0412\, A^{-1} z_e^2 \upsilon_f^{-\frac{9}{10}} D_e^{-\frac{3}{10}} k^{-\frac{2}{5}} \rho_p^{\frac{3}{5}} \phi^{\frac{3}{5}} k_0^{\frac{16}{5}} \left(1 + k_0^3 \phi\right)^{-\frac{3}{5}} (1 + k_0)^{-\frac{1}{5}} \cot\theta \tag{16b}$$

$$k = \frac{(1-\nu_1^2)}{E_1} + \frac{(1-\nu_2^2)}{E_2} \tag{16c}$$

where A is a Hamaker constant, z_e is the effective gap that represents the separation distance between particles and the wall at which the attractive van der Waals forces become significant, ϕ is the packing fraction of the primary particles in the aggregate, ρ_f is the fluid density, D_e is the circular pipe diameter, ν is the Poisson's ratio, E is the Young's modulus, and subscripts 1 and 2 refer to the aggregate and the aerosol particle, respectively. In the calculation the density and viscosity of nitrogen gas are taken for 20 °C. The Hamaker constant between the silica particle and wall separated by nitrogen gas is 1.2×10^{-19} J. The values of k, $\tan\theta$, and ϕ are taken from the literature as 0.1 Pa, 0.3 and 0.25, respectively. For 1 and 2 mm pipes, the values of z_e are considered to be 0.08 and 1 nm, respectively. The

[DOI: 10.1299/mej.23-00423]

constant k_0 is taken as 2 (Theerachaisupakij et al., 2003; Zhu et al., 2012).

4. Model validation using experimental data

4.1 Calculation of DF from the model

Because the aerosol particles have a size distribution, we have a set of aerosol particles with different particle diameters d_i. The decontamination factor DF_i for each particle diameter d_i can be calculated using the model we introduced above. The effective DF can be obtained from Eq. (17) using the aerosol particle size distribution.

$$\mathrm{DF} = \frac{\sum_i (m_{in})_i}{\sum_i \frac{(m_{in})_i}{DF_i}} = \frac{\sum_i \left({d_i}^3 * q_i \right)}{\sum_i \left(\frac{{d_i}^3 * q_i}{DF_i} \right)} \tag{17}$$

where $(m_{in})_i$ is the inlet mass of all aerosol particles, DF_i is the DF for each particle size, and q_i $\left(\sum q_i = 1\right)$ is the number fraction of the aerosol particle with a diameter d_i.

4.2 Comparison of the model data and experimental results

Figures 8 (a) and 8 (b) show the experimentally measured DFs as functions of the flow rate and flow Re number, respectively. The predicted DFs from the Matsui and Murata model (1992) and the present model are also plotted for comparison. Considering the experimental data and the present model, the DF decreases as the flow rate increases and a similar trend is observed as the Re number increases. This may occur because the re-entrainment becomes higher as the flow rate or Re number becomes higher (i.e., deposition decreases).

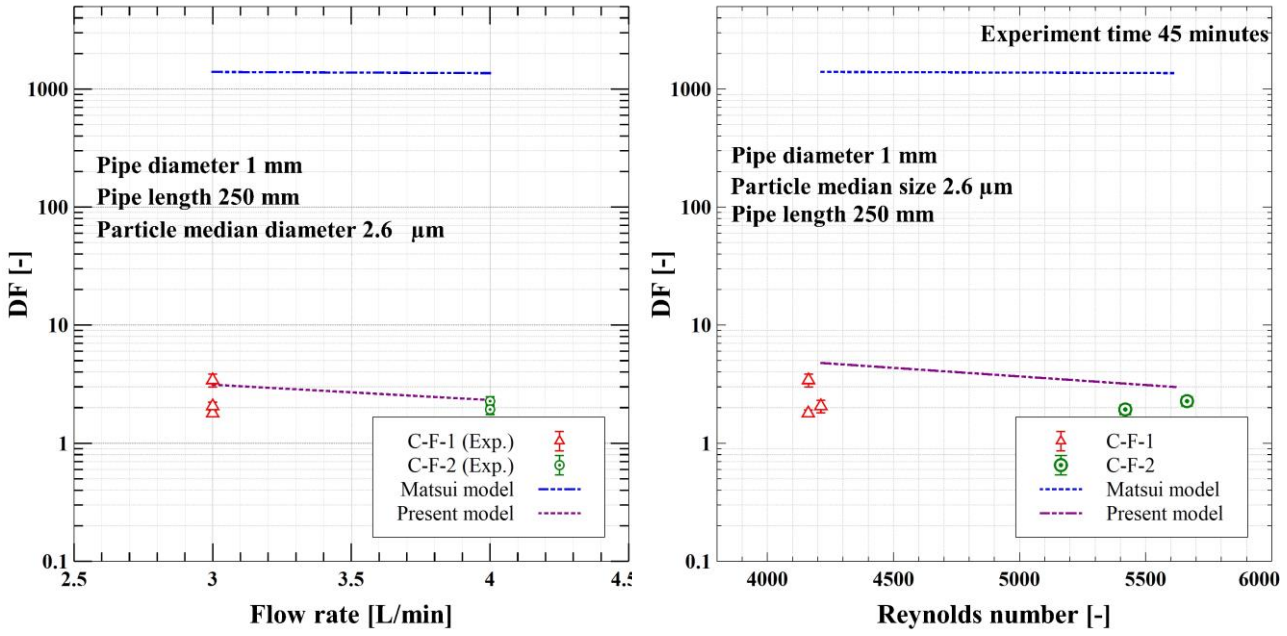

(a) DF versus flow rate for the pipe diameter of 1.0 mm (b) DF versus Re for the pipe diameter of 1.0 mm

Fig. 8 Experimentally obtained DFs and predictions from the Matsui and Murata (1992) model and the present model versus the a) flow rate and b) Reynolds number for a pipe diameter of 1.0 mm.

Figure 9 shows the effect of the median particle diameter on the DFs. Both the Matsui and Murata (1992) model and the experimental results show an increase in DF with the increase in median particle diameter. The present model exhibits the opposite trend but has a similar order of magnitude compared with the experimental DF values. Re-entrainment appears to have a reasonable effect on particle transport and deposition during turbulent flow through a horizontal circular pipe.

[DOI: 10.1299/mej.23-00423]

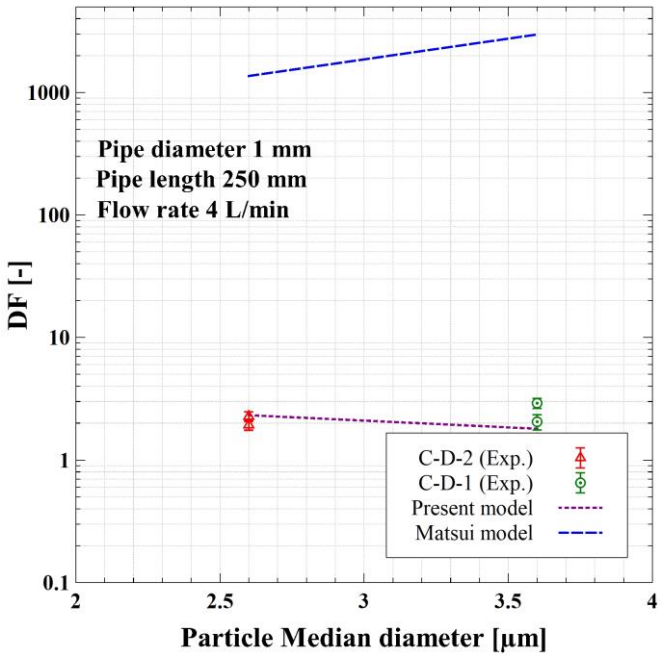

Fig. 9 Experimentally obtained DFs and predictions from the Matsui and Murata (1992) model and the present model versus the median particle diameter for a pipe diameter of 1.0 mm.

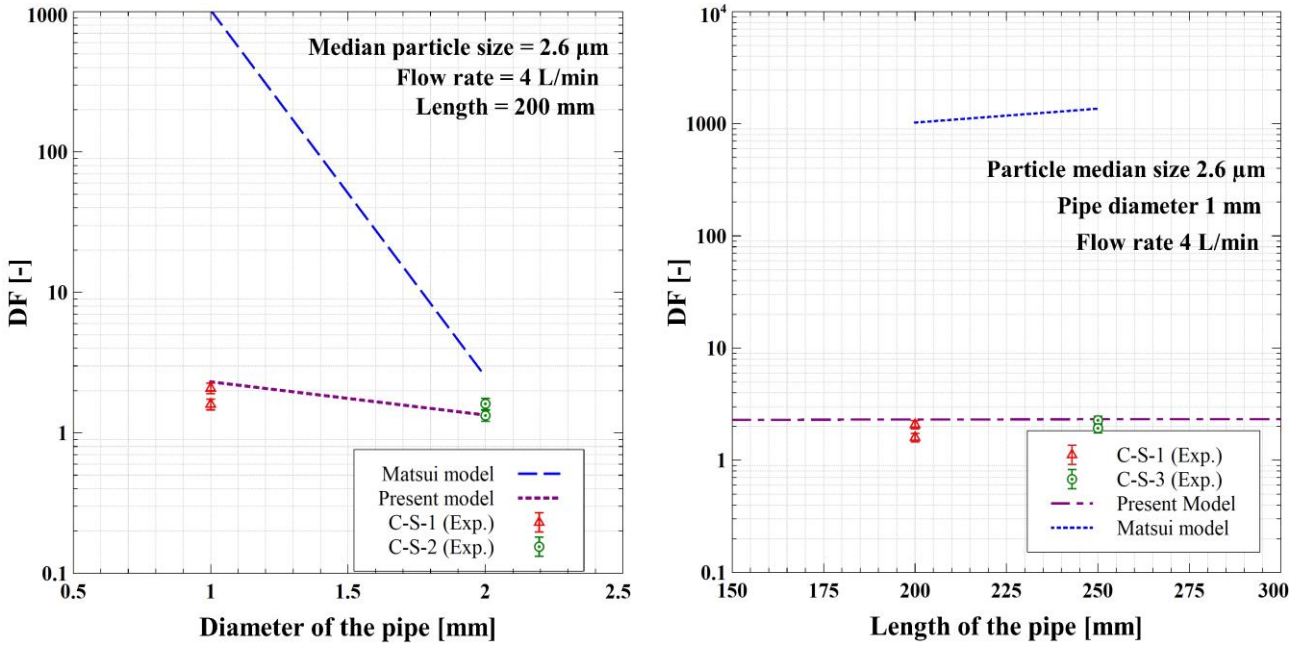

(a) DF versus diameter of the pipe for the pipe length of 200 mm

(b) DF versus length of the pipe for the pipe diameter of 2.0 mm

Fig. 10 Experimentally obtained DFs and predictions from the Matsui and Murata (1992) model and the present model versus the a) pipe diameter for a pipe length of 200 mm and b) pipe length for a pipe diameter of 1.0 mm.

Figures 10 (a) and 10 (b) show the experimentally obtained and predicted DFs for different pipe diameters and pipe lengths, respectively. Figure 10 (a) shows that the DFs decrease as the circular leakage path diameter increases. This may be because the fluid flow velocity decreases as the pipe diameter increases, which results in a decreased turbulence intensity. As the turbulent intensity decreases, the mixing and turbulence of the particles in the fluid flow

[DOI: 10.1299/mej.23-00423]

also decrease, reducing the opportunity for particles to come into contact with the wall. This reduction in the mixing and dispersion can lead to a decrease in the DF with decreasing pipe diameter. Additionally, when the leakage diameter becomes large, the particles need a larger distance to travel to the wall, decreasing the deposition rate (i.e., DF decreases). Moreover, the Matsui and Murata (1992) model becomes more consistent with the experimental results for the 2 mm pipe diameter. This is because the Re is 2809 when the pipe diameter is 2 mm, and in this low Re range, the Matsui and Murata (1992) model prediction matches the experimental results more closely at low Re numbers.

Figure 10 (b) shows that the experimental DFs increase as the leakage flow path length increases. The model prediction also exhibits an increasing trend with the increasing length distribution (150 to 300 mm), although the increase is very small (~0.04), and thus it looks almost constant in the figure. The longer flow path length may result in a higher deposition probability and increase the DFs. Overall, the present model and experimentally obtained DF exhibit similar trends and values.

In the experimental measurement, some errors may come from the measurement of the filter mass using the electronic balance and from the measurement of the flow rate using the flowmeter. The error bars in the experimental results show the standard deviation of the measurements.

5. Conclusion

Test sections and an experimental setup were constructed to collect fundamental data regarding the deposition of FPs within narrow circular pipes that simulate CV penetrations during SAs in NPPs. Aerosol particle deposition experiments were conducted under turbulent flow conditions, and DF data were acquired. From the experimental results, the DF dependences on the pipe length, pipe diameter, flow rate, and particle size are not clear in the measured range; however, the predicted DFs increase with pipe length and decrease with flow rate, particle size, and pipe diameter according to the proposed model. The Matsui and Murata (1992) model for turbulent flow yields significantly higher DF values than those obtained in the experiments, which is attributed to the neglect of aerosol particle re-entrainment in the Matsui and Murata (1992) model. The proposed model accounts for the re-entrainment effect of the deposited particles, and the DFs obtained from this model are more consistent with the experimental results, demonstrating a more accurate representation of the deposition process.

Acknowledgement

This work was supported by a contract research grant from the Central Research Institute of Electric Power Industry (CRIEPI). The authors are grateful to Dr. Koichi Nakamura and Dr. Taizo Kanai for their valuable advice in performing the experiments and assistance in measuring of the particle distributions at CRIEPI.

References

Adhiwidjaja, I., Matsusaka, S., Tanaka, H., and Masuda, H., Simultaneous phenomenon of particle deposition and re-entrainment: effects of surface roughness on deposition layer of striped pattern, Aerosol Science and Technology, Vol. 33, No. 4 (2000), pp. 323–333, DOI:10.1080/02786820050121521.

Allelein, H. J., Auvinen, A., Ball, J., Güntay, S., Herranz, L. E., Hidaka, A., Jones, A. V., Kissane, Martin., Powers, D., and Weber, G., State of the art report on nuclear aerosols, OECD Report NEA/CSNI/R, 5, (2009), (online), available from <https://one.oecd.org/document/NEA/CSNI/R(2009)5/En/pdf>, (accessed on 10 August, 2023).

Cleaver, J. W., and Yates, B., Mechanism of detachment of colloidal particles from a flat substrate in a turbulent flow, Journal of Colloid and Interface Science, Vol. 44, No. 3 (1973), pp. 464–474, DOI:10.1016/0021-9797(73)90323-8.

Friedlander, S. K., and Johnstone, H. F., Deposition of suspended particles from turbulent gas streams, Industrial and Engineering Chemistry, Vol. 49, No. 7 (1957), pp. 1151–1156, DOI:10.1021/ie50571a039.

Kousaka, Y., Okuyama, K., and Endo, Y., Re-entrainment of small aggregate particles from a plane surface by air stream, Journal of Chemical Engineering of Japan, Vol. 13, No.2 (1980), pp. 143–147, DOI:10.1252/jcej.13.143.

Lin, W., Chen, L., Yu, W., Ma, H., Zeng, Z., Lin, J., and Zeng, S., Radioactivity impacts of the Fukushima nuclear

accident on the atmosphere, Atmospheric Environment, Vol. 102 (2015), pp. 311–322, DOI:10.1016/j.atmosenv.2014.11.047.

Liu, B. Y. H., and Ilori, T. A., Aerosol deposition in turbulent pipe flow, Environmental Science and Technology, Vol. 8, No. 4 (1974), pp. 351–356, DOI:10.1021/es60089a001.

Liu, D. L., and Nazaroff, W. W., Particle penetration through building cracks, Aerosol Science and Technology, Vol. 37, No. 7 (2003), pp. 565–573, DOI:10.1080/02786820300927.

Matsui, H., and Murata, M., Deposition of aerosol particles in turbulent pipe flow –the deposition in a horizontal pipe, Journal of Aerosol Research, Vol. 7, No. 3 (1992), pp. 230–239 (in Japanese).

Matsusaka, S., and Masuda, H., Particle re-entrainment from a fine powder layer in a turbulent air flow, Aerosol Science and Technology, Vol. 24, No. 2 (1996), pp. 69–84, DOI:10.1080/02786829608965353.

Morewitz, H. A., Leakage of aerosols from containment buildings, Health Physics, Vol. 42, No. 2 (1982), pp. 195–207, DOI:10.1097/00004032-198202000-00010.

Narayanam, S. P., Kumar, A., Sen, S., Pujala, U., Subramanian, V., Srinivas, C. V., and Baskaran, R., Experimental measurements and theoretical simulation of sodium combustion aerosol leakage through capillaries, Progress in Nuclear Energy, Vol. 118, No. 103111 (2020), DOI:10.1016/j.pnucene.2019.103111.

Parozzi, F., Chatzidakis, S., Gelain, T., Nahas, G., Plumecocq, W., Vendel, J., Herranz, L. E., Hinis, E., Housiadas, C., Journeau, C., Piluso, P., and Malgarida, E., Investigations on aerosol transport in containment cracks, Proceedings of the International Conference on Nuclear Energy for New Europe (2005), pp. 1–10, (online), available from <https://inis.iaea.org/search/search.aspx?orig_q=RN:37104743>, (accessed on 25 July, 2023).

Theerachaisupakij, W., Matsusaka, S., Akashi, Y., and Masuda, H., Re-entrainment of deposited particles by drag and aerosol collision, Journal of Aerosol Science, Vol. 34, No. 3 (2003), DOI: 10.1016/S0021-8502(02)00180-5.

Vate, J. F. V. D., Safety containment buildings as barriers against particulate radioactivity release under accident conditions, Nuclear Technology, Vol. 81, No. 2 (1988), pp. 246–256, DOI:10.13182/NT88-A34095.

Watanabe, A., Yamada, K., and Ohsaki, M., Fission product aerosol trapping effect along the leakage paths of degraded containment penetrations during a severe accident (i) failure criteria of containment penetrations, Transactions of the Atomic Energy Society of Japan, Vol. 8, No. 3, (2009), pp. 254–263, DOI:10.3327/taesj.J08.051.

Zhu, Y., Zhao, B., Zhou, B., and Tan, Z., A particle resuspension model in ventilation ducts, Aerosol Science and Technology, Vol. 46, No. 2 (2012), pp. 222–235, DOI:10.1080/02786826.2011.618471.

Zvoncek, P., Nusbaumer, O., and Torri, A., Development of a fully coupled, all states, all hazards level 2 PSA at leibstadt nuclear power plant, Nuclear Engineering and Technology, Vol. 49, No. 2 (2017), pp. 426–433, DOI:10.1016/j.net.2017.01.016.

[DOI: 10.1299/mej.23-00423]